

Min Yi · Bai-Xiang Xu · Dietmar Gross

Strain-mediated magnetoelectric effect for the electric-field control of magnetic states in nanomagnets

Received: December 27, 2016 / Accepted: date

Abstract Electric-field control of magnetism without electric currents potentially revolutionizes spintronics towards ultralow power. Here by using mechanically coupled phase field simulations, we computationally demonstrate the application of the strain-mediated magnetoelectric effect for the electric-field control of magnetic states in heterostructure. In the model heterostructure constituted of the soft nanomagnet Co and the piezoelectric substrate PMN-PT, both the volatility of magnetic states and the magnetization switching dynamics excited by the electric field are explored. It is found that an electric field can drive the single-domain nanomagnet into an equilibrium vortex state. The nanomagnet remains in the vortex state even after removing the electric field or applying a reverse electric field, i.e. the vortex state is extremely stable and nonvolatile. Only by utilizing the precessional magnetization dynamics, the 180° magnetization switching is possible in small-sized nanomagnets which are free of the stable vortex state. Electric-field pulses can realize the deterministic 180° switching if the electric-field magnitude, pulse width, and ramp time are carefully designed. The minimum switching time is found to be less than 10 ns. These results provide useful information for the design of low-power, reliable, and fast electric-field-controlled spintronics.

Keywords Magnetoelectric effect · Strain mediation · Electric field · Magnetic vortex · 180° switching

1 Introduction

Magnetic systems are promising candidates for the development of fast, high-density, nonvolatile memory technology [1]. Two typical examples of commercial storage systems are magnetic random access memory

M. Yi, B.-X. Xu

Mechanics of Functional Materials Division, Technische Universität Darmstadt, 64287 Darmstadt, Germany

Tel.: +49 6151 16-22922

Fax: +49 6151 16-21034

E-mail: yi@mfm.tu-darmstadt.de; xu@mfm.tu-darmstadt.de

D. Gross

Division of Solid Mechanics, Technische Universität Darmstadt, 64287 Darmstadt, Germany

E-mail: gross@mechanik.tu-darmstadt.de

(MRAM) and spin transfer torque magnetic random access memory (STT-MRAM). Thereby, the magnetic state of nanomagnets is used for the information storage. The switching or writing process is driven by an external magnetic field in MRAM or by a spin-polarized electric current in STT-MRAM. In MRAM, built-in wires in every memory cell are required for the switching of a nanomagnet, i.e. the magnetic field must be generated by passing a current through a wire. The extra wires not only make the device circuit complicated and thus hinder the high density, but also generate current to result in energy dissipation and overheating. In contrast, by using the spin transfer torque effect, STT-MRAM allows for high density. But it is not a low-power method. Usually, a high current density in the order of $10^{10} - 10^{11}$ A/m² [2] is required for the switching of a nanomagnet with an acceptable endurance, leading to high energy dissipation. Therefore, in order to realize the low-power and high-density memory devices, a method without electric currents are ideally desired.

Recently, the control of magnetism by pure electric fields without electric currents provides one viable way for the future low-power next-generation spintronics based memory devices. This strategy can be realized in multiferroic materials which possess more than one ferroic effects and the coupling between two of them. For example, through the magnetoelectric (ME) coupling between the electrical polarization of a ferroelectric material and the magnetization of a ferromagnet, the control of magnetization by an electric field is achievable. Nevertheless, the ME coupling is weak in single phase systems. Such a control is usually implemented through the ME coupling in heterostructures. Generally, in ME heterostructures an electric field can manipulate the magnetization through the interfacial mechanisms such as strain-mediated elastic coupling [3–28], charge modulation [27–38], interface bonding [39–43], and exchanging coupling [20, 44–47]. Since strong elastic coupling between ferroelectric and ferromagnetic phases at room temperature can be achieved across their interfaces, strain-mediated ME effect is one of the most promising candidates and it is thus most extensively investigated in ferromagnetic/ferroelectric heterostructures. In this scenario, a strain generated in a ferroelectric layer by an electric field is transferred to the ferromagnetic layer through the interface and thus controls the magnetization through the magnetoelastic coupling. Due to the long-range nature of the elastic coupling, the strain-mediated ME effect works at the bulk level. On the contrary, all the other three mechanisms are localized to the region near the interface.

In order to establish the strain-mediated ME effect as a feasible strategy in the future practical memory devices driven by electric fields, two technical features should be clarified. Firstly, only if the ferromagnet persists in the new state and does not revert back to the old state after withdraw of the electric field, can this ME effect be applied to memory devices. It means that the magnetic states induced by the electric field should be nonvolatile. Secondly, an electric-field induced deterministic 180° magnetization switching should be achievable, since it determines the reliability and performance of spintronics based memory devices. For example, in order to attain a high signal-to-noise ratio in magnetic tunnel junction (MTJ) for spintronics, a significantly large electric resistance change of MTJ is required, which can only be achieved by a 180° switching in the free layer of MTJ. Trailblazing experiments have demonstrated strain-mediated [14, 38], charge-mediated [35], and exchange-coupling-mediated [46] voltage-driven 180° switching in Ni/BaTiO₃, BiFeO₃-based, and CoFeB/MgO/CoFeB heterostructures, respectively. From the theoretical side, a large number of studies have focused on the strain-mediated 180° switching either by designing the magnet shape [21] or by using the 3D precessional switching dynamics [4–6, 9, 10, 15, 16, 18].

In this work, we study both the volatility of magnetic states and the magnetization switching dynamics excited by the electric field through mechanically coupled phase field simulations. By taking the model heterostructure system which contains the soft nanomagnet Co and the piezoelectric substrate $0.7\text{Pb}(\text{Mg}_{1/3}\text{Nb}_{2/3})\text{O}_3$ - 0.3PbTiO_3 (PMN-PT), we analyze both the equilibrium magnetic states and the precessional dynamic switching process, in order to shed light on how to achieve nonvolatility and 180° switching.

2 Model and simulations

The model heterostructure is shown in Fig. 1, including a nanomagnetic layer Co and a piezoelectric substrate PMN-PT. The nanomagnet is assumed to be much smaller than the substrate so that the strain transferred from the PMN-PT to the Co nanomagnet is nearly uniform. Meanwhile, due to the small magnetostrictive coefficient and small size of Co, the magnetization rotation or switching in Co has little influence on the electromechanical behavior of the piezoelectric substrate. PMN-PT with (011) orientation is used due to its large piezoelectric coefficients $d_{31} = 3175$ pC/N [100] and $d_{32} = 1426$ pC/N $[01\bar{1}]$ [48]. The magnetic state evolution is simulated by a constraint-free phase field model [49, 50]. As shown in Fig. 1, the polar and azimuthal angles (ϑ_1, ϑ_2) instead of the Cartesian components (m_1, m_2, m_3) of the unit magnetization vector are taken as the order parameters. In this way, the constraint of constant magnetization magnitude at the temperature far below the Curie point is fulfilled automatically. The total magnetic enthalpy for the nanomagnet includes the magnetocrystalline anisotropy contribution \mathcal{H}^{ani} , the exchange contribution \mathcal{H}^{exc} , the magnetostatic contribution \mathcal{H}^{mag} , the pure mechanical contribution $\mathcal{H}^{\text{mech}}$, and the magneto-elastic coupling contribution $\mathcal{H}^{\text{mag-ela}}$, i.e.

$$\mathcal{H} = \mathcal{H}^{\text{ani}} + \mathcal{H}^{\text{exc}} + \mathcal{H}^{\text{mag}} + \mathcal{H}^{\text{mech}} + \mathcal{H}^{\text{mag-ela}} \quad (1)$$

in which

$$\begin{aligned} \mathcal{H}^{\text{ani}} &= K_u \sin^2 \vartheta_1 \\ \mathcal{H}^{\text{exc}} &= A_e (\vartheta_{1,j} \vartheta_{1,j} + \sin^2 \vartheta_1 \vartheta_{2,j} \vartheta_{2,j}) \\ \mathcal{H}^{\text{mag}} &= -\frac{1}{2} \mu_0 H_j H_j - \mu_0 M_s (H_1 \sin \vartheta_1 \cos \vartheta_2 + H_2 \sin \vartheta_1 \sin \vartheta_2 + H_3 \cos \vartheta_1) \\ \mathcal{H}^{\text{mech}} &= \frac{1}{2} C_{11} (\varepsilon_{11}^2 + \varepsilon_{22}^2) + \frac{1}{2} C_{33} \varepsilon_{33}^2 + C_{13} (\varepsilon_{11} \varepsilon_{33} + \varepsilon_{22} \varepsilon_{33}) \\ &\quad + C_{12} \varepsilon_{11} \varepsilon_{22} + 2C_{44} (\varepsilon_{23}^2 + \varepsilon_{31}^2) + (C_{11} - C_{12}) \varepsilon_{12}^2 \\ \mathcal{H}^{\text{mag-ela}} &= B_1 (\sin^2 \vartheta_1 \cos^2 \vartheta_2 \varepsilon_{11} + 2 \sin^2 \vartheta_1 \sin 2\vartheta_2 \varepsilon_{12} + \sin^2 \vartheta_1 \sin^2 \vartheta_2 \varepsilon_{22}) \\ &\quad + B_2 \sin^2 \vartheta_1 \varepsilon_{33} + B_3 \sin^2 \vartheta_1 (\varepsilon_{11} + \varepsilon_{22}) \\ &\quad + B_4 (\sin 2\vartheta_1 \sin \vartheta_2 \varepsilon_{23} + \sin 2\vartheta_1 \cos \vartheta_2 \varepsilon_{31}) \end{aligned} \quad (2)$$

Here, C_{11} , C_{12} , C_{33} , C_{13} , and C_{44} are the elastic constants. $\varepsilon_{ij} = \frac{1}{2} (u_{i,j} + u_{j,i})$ are the strain components with u_i as the mechanical displacement. The Latin indices i and j run over 1–3. B_1 , B_2 , B_3 , and B_4 are the magneto-elastic coupling coefficients. K_u is the anisotropy constant. M_s is the saturation magnetization. A_e is the exchange stiffness constant. μ_0 is the vacuum permeability. The magnetic field is expressed as the negative gradient of the magnetic scalar potential ϕ , i.e. $H_j = -\phi_{,j}$.

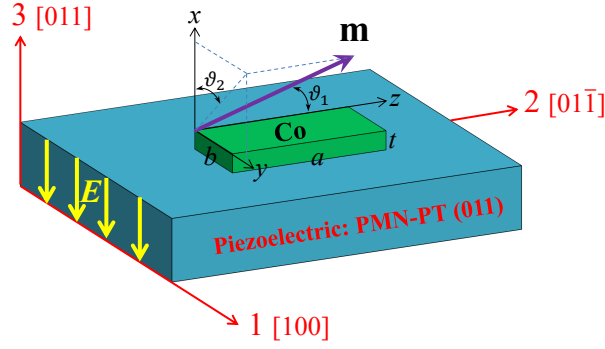


Fig. 1. Model heterostructure containing the nanomagnet Co and the piezoelectric substrate PMN-PT (011).

Based on the above magnetic enthalpy, a combination of the balance law of the configurational force system and the second law of thermodynamics can give rise to a generalized evolution equation for the order parameters ϑ_1 and ϑ_2 , which takes the form [49, 50]:

$$\frac{1}{M_s} \left(\frac{\partial \mathcal{H}}{\partial \vartheta_{\mu,j}} \right)_{,j} - \frac{1}{M_s} \frac{\partial \mathcal{H}}{\partial \vartheta_{\mu}} + \zeta_{\mu}^{\text{ex}} = \frac{1}{\gamma_0} L_{\mu\gamma} \frac{\partial \vartheta_{\gamma}}{\partial t} \quad (3)$$

in which

$$L_{\mu\gamma} = \begin{bmatrix} \alpha & -\sin \vartheta_1 \\ \sin \vartheta_1 & \alpha \sin^2 \vartheta_1 \end{bmatrix}, \quad (4)$$

ζ_{μ}^{ex} is the external driving force for ϑ_1 and ϑ_2 , α the damping coefficient, and $\gamma_0 = 1.76 \times 10^{11} / (Ts)$ the gyromagnetic ratio. The Greek indices μ and γ run over 1–2.

In addition, the mechanical equilibrium equation and the Maxwell equation which governs the magnetic part are incorporated:

$$\left(\frac{\partial \mathcal{H}}{\partial \varepsilon_{ij}} \right)_{,j} = 0 \quad \text{and} \quad \left(-\frac{\partial \mathcal{H}}{\partial H_j} \right)_{,j} = 0 \quad (5)$$

By using the six degrees of freedom $[u_1, u_2, u_3, \phi, \vartheta_1, \vartheta_2]^T$, a three-dimensional nonlinear finite element implementation in FEAP [51] is performed to solve Eqs. (3) and (5). The nanomagnet size is $a = 2b$ and $t = 2$ nm. The materials parameters are taken as [4, 6, 9]: $C_{11}=307$ GPa, $C_{12}=165$ GPa, $C_{44}=75.5$ GPa, $C_{13}=103$ GPa, $C_{33}=358$ GPa, $B_1=-8.1$ MPa, $B_2=-29$ MPa, $B_3=28.2$ MPa, $B_4=29.4$ MPa, $K_u=6.5 \times 10^4$ J/m³, $M_s=1.424 \times 10^6$ A/m, $A_e=3.3 \times 10^{-11}$ J/m, $\alpha=0.01$. Due to the exchange length $\sqrt{2A_e/(\mu_0 M_s^2)} \approx 5.1$ nm, the finite element mesh size is chosen to be 2 nm. The strain generated by applying an electric field to the PMN-PT is estimated as $\varepsilon_{yy} = Ed_{31}$ and $\varepsilon_{zz} = Ed_{32}$ in the nanomagnet Co, as shown in Fig. 1

3 Results and discussions

3.1 Electric field induced nonvolatile vortex states

From the viewpoint of information storage such as binary logic and memory applications, the magnetic states triggered by an electric field should be nonvolatile. This requires that the magnetic states should be robustly kept after the removal of the electric field. As the first step, we explore the electric field induced equilibrium

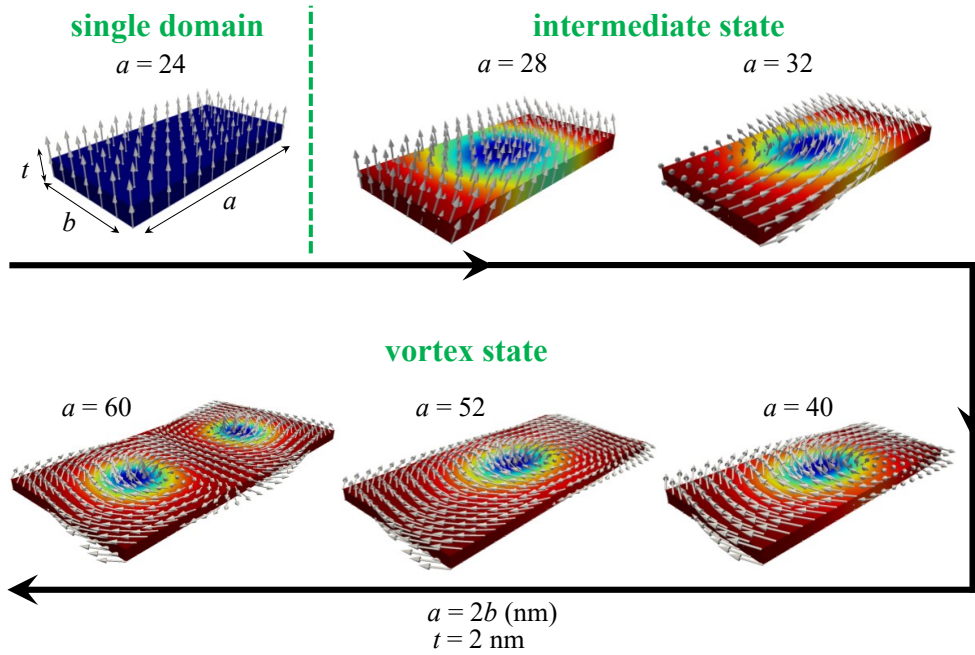


Fig. 2. Equilibrium magnetic states varying with the nanomagnet size in the case of $E = 7 \text{ kV/cm}$.

magnetic states, in order to figure out whether the nonvolatile state is achievable when the electric field is applied for a sufficient long time without a precise control of time. The initial state is a single domain along the z axis (Fig. 1). Then an electric field is applied to drive the initial state into another magnetic state. Fig. 2 presents the equilibrium magnetic states when an electric field of $E = 7 \text{ kV/cm}$ is applied. It can be found that the electric field induced equilibrium magnetic states are dependent on the nanomagnet size. If the size is small (e.g. $a = 24 \text{ nm}$), a single-domain state survives with the magnetization perpendicular to the plane. Such a state possesses high magnetostatic energy and magnetocrystalline anisotropy energy, but low magneto-elastic energy. The role of the latter energy surpasses that of the former two energies in the small-sized sample, thus leading to a single domain. On the contrary, in the case of large size (e.g. $a = 52 \text{ nm}$), we attain a vortex structure in which the magnetization near the vortex core gradually tilts out of plane. The vortex is a result of substantially reducing the exchange energy and slightly increasing the magnetostatic energy and the magnetocrystalline anisotropy energy. In the region outside the vortex, the magnetization almost lies in the plane due to the dominating role of the magnetostatic energy. When the in-plane size is large, the magnetostatic energy will be very large if the magnetization deviates from the plane. If the in-plane size is neither too small nor too large (e.g. $a = 32 \text{ nm}$), the magnetostatic energy and the magneto-elastic energy are comparable. Then we have an intermediate state, in which neither single domain nor perfect vortex state exists. All the magnetization tilts out of the plane and only presents the trend of forming a vortex state. These results provide fruitful insight onto the electric-field control of magnetic states by tuning the nanomagnet size.

It should be noted that the magnetic states shown in Fig. 2 are achieved when a constant electric field is always kept. The stability of these magnetic states should be further examined. For example, in the case of equilibrium single domain (e.g. $a = 24 \text{ nm}$), we find that after removing the electric field, the magnetization will either revert back to the initial state or switch to the negative z axis. It indicates a volatile state. While

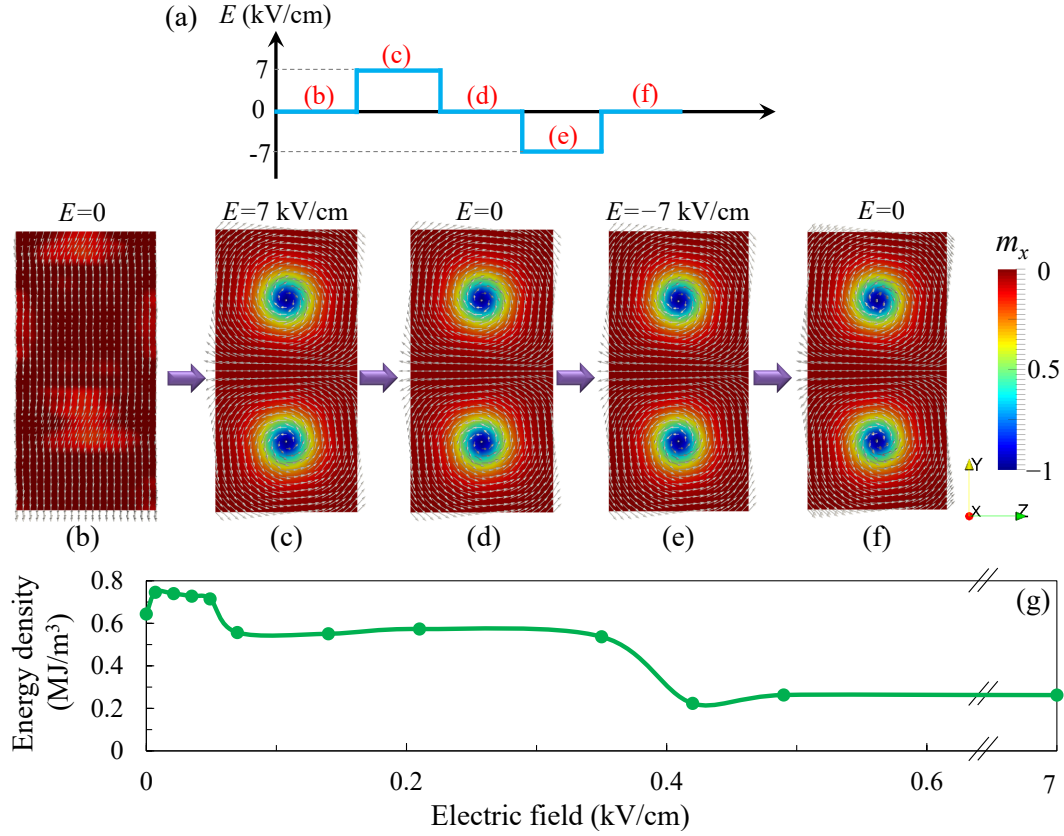


Fig. 3. The evolution of equilibrium magnetic states (b)-(f) in a nanomagnet when the electric field history in (a) is applied. (g) Total energy related to magnetization as a function of electric field. $a = 2b = 80$ nm, $t = 2$ nm.

the intermediate and vortex states can remain after the removal of the electric field and show nonvolatility. Fig. 3(b)-(f) presents the typical vortex state evolution in the case of an alternating electric field shown in Fig. 3(a). For every stage in Fig. 3(a), the electric field duration is long enough to make the magnetization reach the equilibrium state. Based on the initial single-domain state in Fig. 3(b), we find that the magnetic state transforms to the vortex state in Fig. 3(c) by applying an electric field of 7 kV/cm. This vortex state remains as the electric field vanishes in Fig. 3(d). A negative electric field of -7 kV/cm is subsequently applied, but it does not push the nanomagnet out of the vortex state, as shown in Fig. 3(e). Eventually, after removing the negative electric field again, the vortex state continues to remain (Fig. 3(f)). These features clearly demonstrate the nonvolatile vortex state. A similar vortex state, driven by acoustic waves, was also observed in elliptical cobalt nanomagnets in recent experiments [52].

Both the vortex state and the initial single-domain state are local energy minima. But in order to get the vortex state from the initial single-domain state, the nanomagnet has to experience the state with high exchange energy so that the formation of a curling magnetic structure is possible. Therefore, an energy barrier exists between these two states. When this energy barrier is overcome by the magneto-elastic energy which is introduced from the electric field, the magnetization will be driven from the initial single-domain state into the vortex state. Moreover, due to its local minimum, the vortex state can persist after the removal of the electric

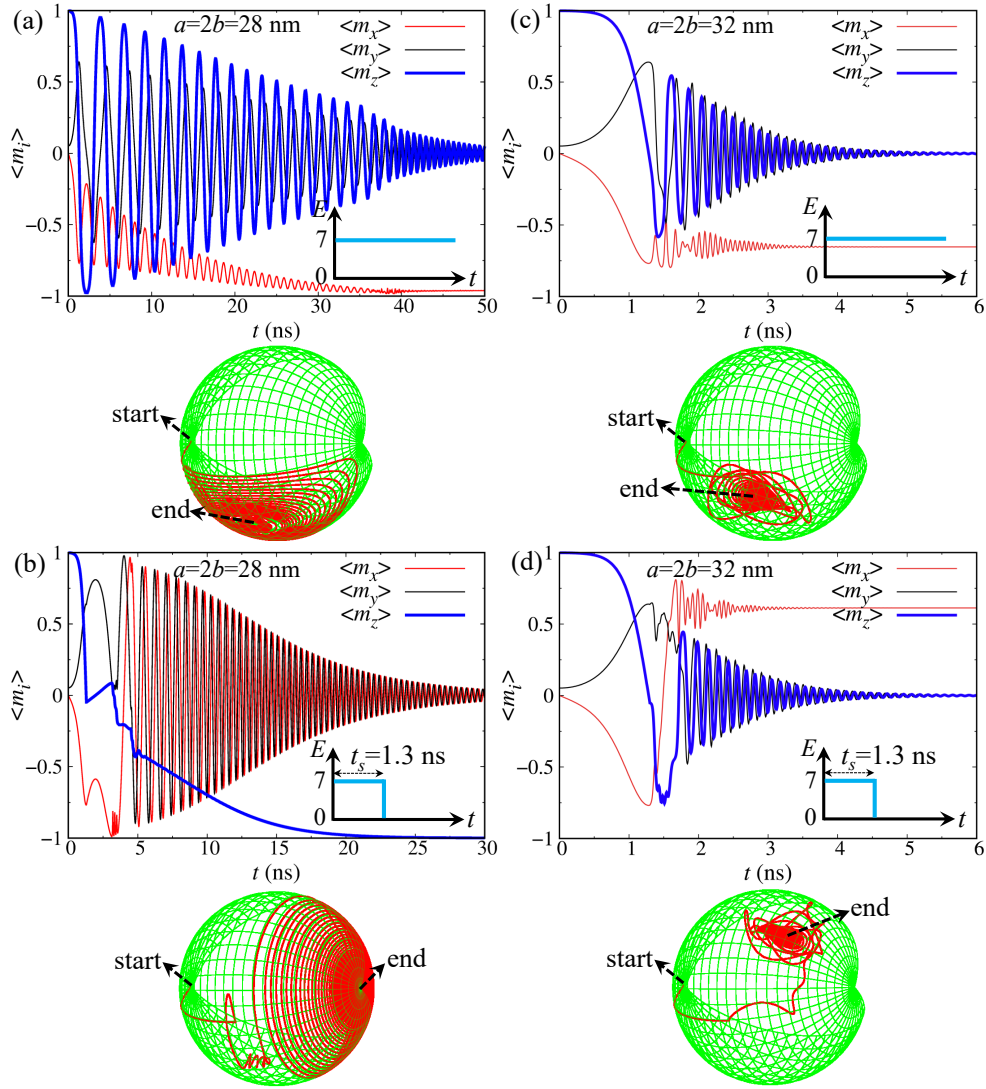


Fig. 4. Dynamics of average magnetization components $\langle m_i \rangle$. An electric field of 7 kV/cm is always kept for the nanomagnet with (a) $a = 2b = 28$ nm and (c) $a = 2b = 32$ nm. An electric field of 7 kV/cm with a pulse width of 1.3 ns is applied for the nanomagnet with (b) $a = 2b = 28$ nm and (d) $a = 2b = 32$ nm.

field. This explains the transition from Fig. 3(b) to Fig. 3(d). In addition, since the vortex state is extremely stable, the electric field is obviously not sufficient to drive the magnetization out of the vortex state. This can be verified by Fig. 3(c)-(f), in which the vortex state presents little difference no matter the electric field is 7, 0, or -7 kV/cm. Only a magnetic field is possible to restore the initial single-domain state in Fig. 3(b). The evolution of energy density (related to magnetization) in Fig. 3(g) shows that a small electric field is required to drive the initial single-domain state into a magnetic curling state, along with an increase in the energy density. Then an electric field around 0.5 kV/cm is enough to stimulate the stable vortex state. The stable and nonvolatile vortex state paves an alternative way for designing memory devices.

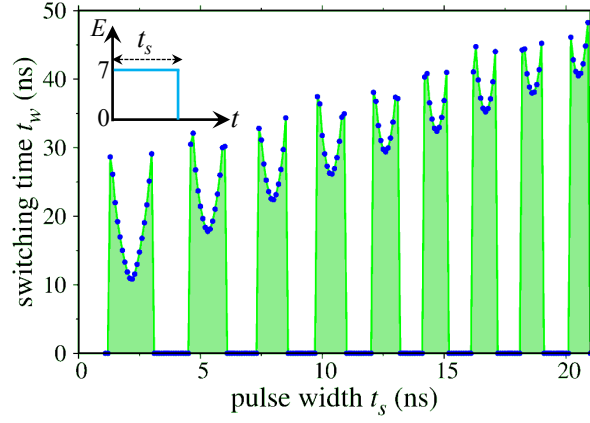


Fig. 5. 180° switching time t_w as a function of pulse width t_s ($E = 7$ kV/cm, $t_r = 0$). In the regions between the green columns a 180° switching is unachievable.

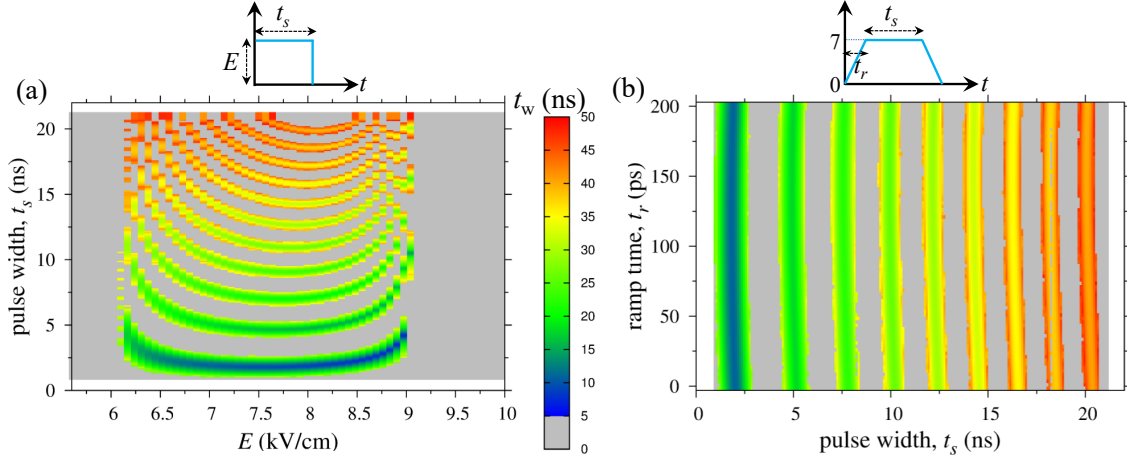


Fig. 6. 180° switching time t_w (a) as a function of electric field magnitude E and pulse width t_s ($t_r = 0$), and (b) as a function of pulse width t_s and ramp time t_r . The gray region means 180° switching unachievable.

3.2 Electric field induced 180° switching

The above study, focusing on the equilibrium magnetic states, implies that none of the nanomagnets experience a deterministic complete reversal of magnetization, i.e. 180° switching which also plays an important role in the spintronics based memory devices. How to achieve a 180° switching purely by an electric field is critical for the design of low-power spintronics. In contrast to the above study, here we apply an electric field pulse to trigger the 180° switching by utilizing the precessional magnetization dynamics. Fig. 4 presents the typical results for the temporal evolution of average magnetization components for two nanomagnets with different size. It can be found in Fig. 4(a) and (c) that for both nanomagnets, new magnetic states similar to those in Fig. 2 are formed if the electric field is always kept. No 180° switching occurs. However, if we apply an electric field pulse, the 180° switching is possible, as shown in Fig. 4(b) for the nanomagnet with a size of $a = 2b = 28$ nm. But if the nanomagnet size is increased to $a = 2b = 32$ nm, even an electric field

pulse cannot achieve a 180° switching, as shown in Fig. 4(d). Such results indicate that the achievement of 180° switching relies on the nanomagnet size. Larger size implies a magnetization state more close to a vortex-like curling structure which is more stable (Fig. 2), thus prohibiting the 180° switching. Only in the case of relatively small size where magnetization is close to coherent rotation, a 180° switching is achievable if the precessional dynamics is utilized. In order to confirm the above size dependence, we perform a series of simulations for the size not smaller than $a = 2b = 32$ nm. It is found that, no matter how to control the electric field magnitude and pulse width, a 180° switching is seldom obtainable. It is absolutely impossible to achieve the 180° switching in the size range ($a > \sim 40$ nm) for the equilibrium vortex state in Fig. 2. In the case of size range ($a < \sim 24$ nm) for the single-domain state in Fig. 2, exactly coherent switching occurs and a 180° switching can be definitely achieved by controlling the electric field pulse. In the case of size range ($24 \text{ nm} < a < 40 \text{ nm}$) for the intermediate state in Fig. 2, a 180° switching is possible for the size close to the single-domain region but impossible for the size close the vortex region.

After confirming the feasibility of achieving 180° switching through the precessional magnetization dynamics, we further study the effect of electric field magnitude, pulse width (t_s), and ramp time (t_r) on the switching behavior in the nanomagnet with $a = 2b = 28$ nm. Fig. 5(a) presents the switching time (t_w) as a function of t_s in the case of $E = 7$ kV/cm and $t_r = 0$. It exhibits intermittent pulse-width regions (filled by green color) for the 180° switching events, inheriting the nature of precessional dynamics and oscillated behavior (e.g. Fig. 4(a) and (b)). In each intermittent region, a local minimum switching time can be determined, which increases with the pulse width. In the case of $t_s = 2.2$ ns, a global minimum switching time of ~ 10 ns can be realized. These results inspire a careful design of pulse width to develop a fast switching and fast memory technology.

We further manipulate all the electric field magnitude, pulse width, and ramp time to give a systematic insight onto the 180° switching condition and the switching time, as shown in Fig. 6. It can be found from Fig. 6(a) that the minimum electric field for a 180° switching is around 6.1 kV/cm and the maximum is around 9 kV/cm. In order to achieve a 180° switching, both the electric field magnitude and pulse width should be carefully designed. In the case of $E \sim 8.9$ kV/cm and $t_s = 3.7$ ns, a fast switching with $t_w \sim 7.4$ ns can be realized. We also consider that the electric field is not applied instantly, i.e. a ramp time is required to increase E from 0 to the final magnitude, as shown in Fig. 6(b). It is found that the ramp time t_r within 200 ps has no strong influence on the switching time. For all the cases in Fig. 6, a 180° switching within less than 10 ns is attainable. It should be noted that the switching time of < 10 ns here is close to that in the traditional STT-MRAM, MRAM, and DRAM (dynamic random access memory) [53], but without any electric currents.

4 Conclusions

The electric-field control of magnetic states in nanomagnets by the strain-mediated magnetoelectric effect in nanomagnetic/piezoelectric heterostructure has been studied by phase field simulations. It is found that depending on the nanomagnet size, the electric field induced equilibrium magnetic states can be either non-volatile or volatile. For large nanomagnet size, a nonvolatile vortex states can be achieved, which persists after removing the electric field or applying a reverse electric field. For small nanomagnet size, coherent switching occurs and the electric field induced single-domain state is unstable and volatile. For the nanomagnet

size between the above two cases, an intermediate magnetic state between single domain and vortex exists. By using the precessional magnetization dynamics in the case of single-domain state and intermediate state which is close to the single-domain state, a 180° switching can be achieved by an electric field pulse. On the contrary, for the case of vortex state and intermediate state which is close to the vortex state, a 180° switching is impossible. Careful design of the electric field magnitude, pulse width, and ramp time can result in a 180° switching time of less than 10 ns, which is close to that in the traditional STT-MRAM, MRAM, and DRAM. It is anticipated that the present study provides valuable insight into the design of electric-field control of non-volatile magnetic states and 180° switching without electric currents for achieving low-power, high-speed, nonvolatile, and highly compact memory devices.

Acknowledgements The financial supports from the German federal state of Hessen through its excellence programme LOEWE RESPONSE and the German Science Foundation (individual project Xu 121/7-1 and the project Xu 121/4-2 in the Forschergruppe FOR1509) are appreciated. The authors also greatly acknowledge the access to the Lichtenberg High Performance Computer of TU Darmstadt.

References

1. Salahuddin, S., Datta, S.: Interacting systems for self-correcting low power switching. *Appl Phys Lett* 90(9), 093503 (2007). doi:10.1063/1.2709640
2. Katine, J.A., Albert, F.J., Buhrman, R.A., Myers, E.B., Ralph, D.C.: Current-driven magnetization reversal and spin-wave excitations in Co/Cu/Co pillars. *Phys Rev Lett* 84(14), 3149-3152 (2000). doi:10.1103/PhysRevLett.84.3149
3. Peng, R.C., Hu, J.M., Momeni, K., Wang, J.J., Chen, L.Q., Nan, C.W.: Fast 180° magnetization switching in a strain-mediated multiferroic heterostructure driven by a voltage. *Sci Rep* 6, 27561 (2016). doi:10.1038/srep27561
4. Yi, M., Xu, B.-X., Shen, Z.: Effects of magnetocrystalline anisotropy and magnetization saturation on the mechanically induced switching in nanomagnets. *J Appl Phys* 117(10), 103905 (2015). doi:10.1063/1.4914485
5. Hu, J.M., Yang, T., Wang, J., Huang, H., Zhang, J., Chen, L.Q., Nan, C.W.: Purely electric-field-driven perpendicular magnetization reversal. *Nano Lett* 15(1), 616-622 (2015). doi:10.1021/nl504108m
6. Yi, M., Xu, B.-X., Shen, Z.: 180° magnetization switching in nanocylinders by a mechanical strain. *Extreme Mech Lett* 3, 66-71 (2015). doi:10.1016/j.eml.2015.03.004
7. Wang, J., Hu, J., Wang, H., Jiang, H., Wu, Z., Ma, J., Wang, X., Lin, Y., Nan, C.W.: Electric-field modulation of magnetic properties of Fe films directly grown on BiScO₃-PbTiO₃ ceramics. *J Appl Phys* 107(8), 083901 (2010). doi:10.1063/1.3369284
8. Liu, M., Nan, T., Hu, J.-M., Zhao, S.-S., Zhou, Z., Wang, C.-Y., Jiang, Z.-D., Ren, W., Ye, Z.-G., Chen, L.-Q., Sun, N.X.: Electrically controlled non-volatile switching of magnetism in multiferroic heterostructures via engineered ferroelastic domain states. *NPG Asia Mater* 8(9), e316 (2016). doi:10.1038/am.2016.139
9. Yi, M., Xu, B.-X., Gross, D.: Mechanically induced deterministic 180° switching in nanomagnets. *Mech Mater* 87, 40-49 (2015). doi:10.1016/j.mechmat.2015.04.006

10. Hu, J.-M., Yang, T.N., Chen, L.Q., Nan, C.W.: Voltage-driven perpendicular magnetic domain switching in multiferroic nanoislands. *J Appl Phys* 113(19), 194301 (2013). doi:10.1063/1.4804157
11. Hu, J.-M., Nan, C.W.: Electric-field-induced magnetic easy-axis reorientation in ferromagnetic/ferroelectric layered heterostructures. *Phys Rev B* 80(22) (2009). doi:10.1103/PhysRevB.80.224416
12. Buzzi, M., Chopdekar, R.V., Hockel, J.L., Bur, A., Wu, T., Pilet, N., Warnicke, P., Carman, G.P., Heyderman, L.J., Nolting, F.: Single domain spin manipulation by electric fields in strain coupled artificial multiferroic nanostructures. *Phys Rev Lett* 111(2), 027204 (2013). doi:10.1103/PhysRevLett.111.027204
13. Ghidini, M., Maccherozzi, F., Moya, X., Phillips, L.C., Yan, W., Soussi, J., Metallier, N., Vickers, M.E., Steinke, N.J., Mansell, R., Barnes, C.H., Dhesi, S.S., Mathur, N.D.: Perpendicular local magnetization under voltage control in Ni films on ferroelectric BaTiO₃ substrates. *Adv Mater* 27(8), 1460-1465 (2015). doi:10.1002/adma.201404799
14. Ghidini, M., Pellicelli, R., Prieto, J.L., Moya, X., Soussi, J., Briscoe, J., Dunn, S., Mathur, N.D.: Non-volatile electrically-driven repeatable magnetization reversal with no applied magnetic field. *Nat Commun* 4, 1453 (2013). doi:10.1038/ncomms2398
15. Roy, K., Bandyopadhyay, S., Atulasimha, J.: Binary switching in a 'symmetric' potential landscape. *Sci Rep* 3, 3038 (2013). doi:10.1038/srep03038
16. Roy, K., Bandyopadhyay, S., Atulasimha, J.: Switching dynamics of a magnetostrictive single-domain nanomagnet subjected to stress. *Phys Rev B* 83(22) (2011). doi:10.1103/PhysRevB.83.224412
17. Tiercelin, N., Dusch, Y., Klimov, A., Giordano, S., Preobrazhensky, V., Pernod, P.: Room temperature magnetoelectric memory cell using stress-mediated magnetoelastic switching in nanostructured multilayers. *Appl Phys Lett* 99(19), 192507 (2011). doi:10.1063/1.3660259
18. Roy, K., Bandyopadhyay, S., Atulasimha, J.: Energy dissipation and switching delay in stress-induced switching of multiferroic nanomagnets in the presence of thermal fluctuations. *J Appl Phys* 112(2), 023914 (2012). doi:10.1063/1.4737792
19. Brintlinger, T., Lim, S.H., Baloch, K.H., Alexander, P., Qi, Y., Barry, J., Melngailis, J., Salamanca-Riba, L., Takeuchi, I., Cumings, J.: In situ observation of reversible nanomagnetic switching induced by electric fields. *Nano Lett* 10(4), 1219-1223 (2010). doi:10.1021/nl9036406
20. Wang, J.J., Hu, J.M., Yang, T.N., Feng, M., Zhang, J.X., Chen, L.Q., Nan, C.W.: Effect of strain on voltage-controlled magnetism in BiFeO₃-based heterostructures. *Sci Rep* 4, 4553 (2014). doi:10.1038/srep04553
21. Wang, J.J., Hu, J.M., Ma, J., Zhang, J.X., Chen, L.Q., Nan, C.W.: Full 180 degrees magnetization reversal with electric fields. *Sci Rep* 4, 7507 (2014). doi:10.1038/srep07507
22. Li, P., Chen, A., Li, D., Zhao, Y., Zhang, S., Yang, L., Liu, Y., Zhu, M., Zhang, H., Han, X.: Electric field manipulation of magnetization rotation and tunneling magnetoresistance of magnetic tunnel junctions at room temperature. *Adv Mater* 26(25), 4320-4325 (2014). doi:10.1002/adma.201400617
23. Avakian, A., Gellmann, R., Ricoeur, A.: Nonlinear modeling and finite element simulation of magnetoelectric coupling and residual stress in multiferroic composites. *Acta Mech* 226(8), 2789-2806 (2015). doi:10.1007/s00707-015-1336-0
24. Ezzin, H., Amor, M.B., Ghazlen, M.H.B.: Propagation behavior of SH waves in layered piezoelectric/piezomagnetic plates. *Acta Mech* (2016). doi:10.1007/s00707-016-1744-9

25. Sridhar, A., Keip, M.-A., Miehe, C.: Homogenization in micro-magneto-mechanics. *Comput Mech* 58(1), 151-169 (2016). doi: 10.1007/s00466-016-1286-y
26. Wang, J., Li, G.-P., Shimada, T., Fang, H., Kitamura, T.: Control of the polarity of magnetization vortex by torsion. *Appl Phys Lett* 103(24), 242413 (2016). doi:10.1063/1.4847375
27. Ong, P.V., Kioussis, N., Odkhuu, D., Amiri, P.K., Wang, K.L., Carman, G. P.: Giant voltage modulation of magnetic anisotropy in strained heavy metal/magnet/insulator heterostructures. *Phys Rev B* 92(2), 020407(R) (2015). doi:10.1103/PhysRevB.92.020407
28. Ong, P.V., Kioussis, N., Amiri, P.K., Wang, K.L.: Electric-field-driven magnetization switching and nonlinear magnetoelasticity in Au/FeCo/MgO heterostructures. *Sci Rep* 6, 29815 (2016). doi:10.1038/srep29815
29. Weisheit, M., Fahler, S., Marty, A., Souche, Y., Poinson, C., Givord, D.: Electric field-induced modification of magnetism in thin-film ferromagnets. *Science* 315(5810), 349-351 (2007). doi:10.1126/science.1136629
30. Zhu, W., Xiao, D., Liu, Y., Gong, S.J., Duan, C.G.: Picosecond electric field pulse induced coherent magnetic switching in MgO/FePt/Pt(001)-based tunnel junctions: a multiscale study. *Sci Rep* 4, 4117 (2014). doi:10.1038/srep04117
31. Rondinelli, J.M., Stengel, M., Spaldin, N.A.: Carrier-mediated magnetoelectricity in complex oxide heterostructures. *Nat Nanotechnol* 3(1), 46-50 (2008). doi:10.1038/nnano.2007.412
32. Duan, C.G., Velez, J.P., Sabirianov, R.F., Zhu, Z., Chu, J., Jaswal, S.S., Tsymbal, E.Y.: Surface magnetoelectric effect in ferromagnetic metal films. *Phys Rev Lett* 101(13), 137201 (2008). doi:10.1103/PhysRevLett.101.137201
33. Maruyama, T., Shiota, Y., Nozaki, T., Ohta, K., Toda, N., Mizuguchi, M., Tulapurkar, A.A., Shinjo, T., Shiraishi, M., Mizukami, S., Ando, Y., Suzuki, Y.: Large voltage-induced magnetic anisotropy change in a few atomic layers of iron. *Nat Nanotechnol* 4(3), 158-161 (2009). doi:10.1038/nnano.2008.406
34. Niranjana, M.K., Duan, C.-G., Jaswal, S.S., Tsymbal, E.Y.: Electric field effect on magnetization at the Fe/MgO(001) interface. *Appl Phys Lett* 96(22), 222504 (2010). doi:10.1063/1.3443658
35. Wang, W.G., Li, M., Hageman, S., Chien, C.L.: Electric-field-assisted switching in magnetic tunnel junctions. *Nat Mater* 11(1), 64-68 (2011). doi:10.1038/nmat3171
36. Shiota, Y., Nozaki, T., Bonell, F., Murakami, S., Shinjo, T., Suzuki, Y.: Induction of coherent magnetization switching in a few atomic layers of FeCo using voltage pulses. *Nat Mater* 11(1), 39-43 (2011). doi:10.1038/nmat3172
37. Zhou, Z., Howe, B.M., Liu, M., Nan, T., Chen, X., Mahalingam, K., Sun, N.X., Brown, G.J.: Interfacial charge-mediated non-volatile magnetoelectric coupling in $\text{Co}_{0.3}\text{Fe}_{0.7}/\text{Ba}_{0.6}\text{Sr}_{0.4}\text{TiO}_3/\text{Nb:SrTiO}_3$ multiferroic heterostructures. *Sci Rep* 5, 7740 (2015). doi:10.1038/srep07740
38. Yang, S.W., Peng, R.C., Jiang, T., Liu, Y.K., Feng, L., Wang, J.J., Chen, L.Q., Li, X.G., Nan, C.W.: Non-volatile 180 degrees magnetization reversal by an electric field in multiferroic heterostructures. *Adv Mater* 26(41), 7091-7095 (2014). doi:10.1002/adma.201402774
39. Duan, C.G., Jaswal, S.S., Tsymbal, E.Y.: Predicted magnetoelectric effect in Fe/BaTiO₃ multilayers: ferroelectric control of magnetism. *Phys Rev Lett* 97(4), 047201 (2006). doi:10.1103/PhysRevLett.97.047201

40. Fechner, M., Maznichenko, I.V., Ostanin, S., Ernst, A., Henk, J., Bruno, P., Mertig, I.: Magnetic phase transition in two-phase multiferroics predicted from first principles. *Phys Rev B* 78(21) (2008). doi:10.1103/PhysRevB.78.212406
41. Duan, C.-G., Veleev, J.P., Sabirianov, R.F., Mei, W.N., Jaswal, S.S., Tsymbal, E.Y.: Tailoring magnetic anisotropy at the ferromagnetic/ferroelectric interface. *Appl Phys Lett* 92(12), 122905 (2008). doi:10.1063/1.2901879
42. Yamauchi, K., Sanyal, B., Picozzi, S.: Interface effects at a half-metal/ferroelectric junction. *Appl Phys Lett* 91(6), 062506 (2007). doi:10.1063/1.2767776
43. Duan, C.G., Sabirianov, R.F., Mei, W.N., Jaswal, S.S., Tsymbal, E.Y.: Interface effect on ferroelectricity at the nanoscale. *Nano Lett* 6(3), 483-487 (2006). doi:10.1021/nl0524521
44. Fechner, M., Zahn, P., Ostanin, S., Bibes, M., Mertig, I.: Switching magnetization by 180 degrees with an electric field. *Phys Rev Lett* 108(19), 197206 (2012). doi:10.1103/PhysRevLett.108.197206
45. Chu, Y.H., Martin, L.W., Holcomb, M.B., Gajek, M., Han, S.J., He, Q., Balke, N., Yang, C.H., Lee, D., Hu, W., Zhan, Q., Yang, P.L., Fraile-Rodriguez, A., Scholl, A., Wang, S.X., Ramesh, R.: Electric-field control of local ferromagnetism using a magnetoelectric multiferroic. *Nat Mater* 7(6), 478-482 (2008). doi:10.1038/nmat2184
46. Heron, J.T., Bosse, J.L., He, Q., Gao, Y., Trassin, M., Ye, L., Clarkson, J.D., Wang, C., Liu, J., Salahuddin, S., Ralph, D.C., Schlom, D.G., Iiguez, J., Huey, B.D., Ramesh, R.: Deterministic switching of ferromagnetism at room temperature using an electric field. *Nature* 516(7531), 370-373 (2014). doi:10.1038/nature14004
47. Wang, J.J., Hu, J.M., Peng, R.C., Gao, Y., Shen, Y., Chen, L.Q., Nan, C.W.: Magnetization reversal by out-of-plane voltage in BiFeO₃-based multiferroic heterostructures. *Sci Rep* 5, 10459 (2015). doi:10.1038/srep10459
48. Peng, J., Luo, H.-s., Lin, D., Xu, H.-q., He, T.-h., Jin, W.-q.: Orientation dependence of transverse piezoelectric properties of 0.70Pb(Mg_{1/3}Nb_{2/3})O₃-0.30PbTiO₃ single crystals. *Appl Phys Lett* 85(25), 6221 (2004). doi:10.1063/1.1839288
49. Yi, M., Xu, B.-X.: A real-space and constraint-free phase field model for the microstructure of ferromagnetic shape memory alloys. *Int J Fract* 202(2), 179-194 (2016). doi:10.1007/s10704-016-0152-4
50. Yi, M., Xu, B.X.: A constraint-free phase field model for ferromagnetic domain evolution. *Proc R Soc A* 470(2171), 20140517 (2014). doi:10.1098/rspa.2014.0517
51. Taylor, R.L.: FEAP-A finite element analysis program. <http://www.ce.berkeley.edu/projects/feap/>.
52. Sampath, V., D'Souza, N., Bhattacharya, D., Atkinson, G.M., Bandyopadhyay, S., Atulasimha, J.: Acoustic-wave-induced magnetization switching of magnetostrictive nanomagnets from single-Domain to nonvolatile vortex states. *Nano Lett* 16(9), 5681-5687 (2016). doi:10.1021/acs.nanolett.6b02342
53. Wang, K.L., Alzate, J.G., Khalili Amiri, P.: Low-power non-volatile spintronic memory: STT-RAM and beyond. *J Phys D Appl Phys* 46(7), 074003 (2013). doi:10.1088/0022-3727/46/7/074003